Journal of Materials Chemistry C

PAPER

View Article Online
View Journal | View Issue

Cite this: J. Mater. Chem. C, 2019, 7, 3607

Junction-configuration-dependent interfacial electronic states of a monolayer MoS_2/metal contact†

Qinglong Fang,[a] Xumei Zhao,[b] Yuhong Huang,[c] Kewei Xu,[ad] Tai Min[a] and Fei Ma*[a]

Received 30th August 2018,
Accepted 18th February 2019

DOI: 10.1039/c8tc04341h

rsc.li/materials-c

Electrical contacts are crucial to the high performances of electronic devices, and they become more prominent for the popular two-dimensional (2D) semiconductors because they commonly have high contact resistances and are sensitive to the interfacial states. In this paper, taking monolayer MoS_2 as an example, first-principles calculations are done to study and predict the influences of the contact mode on the interfacial electronic states of monolayer MoS_2/metal (metal = Mg, Al, In, Cu, Ag, Au, Pd, Sc, and Ti). It is found that the interfacial properties are determined by the matching degree between the electronic states of the monolayer MoS_2 and metal electrodes. The top contact configuration is preferred for the monolayer MoS_2/Sc system as a result of an extremely low Schottky barrier (0.086 eV) as compared to that (0.439 eV) in the edge contact configuration, however, the edge contact configuration is preferred for Ag, Cu, Au, and Pd electrodes. Furthermore, metal electrodes in the top contact configuration might usually result in n-type doping of monolayer MoS_2, but lead to p-type doping in the edge contact configuration. The pinning factor S (0.257, −0.009, −0.132, and −0.172) of monolayer MoS_2 in both contact modes is close to zero, suggesting a strong electronic pinning effect. The findings provide theoretical guidance for the selection of electrodes for high-performance 2D material based devices.

1. Introduction

Over the last decade, a great number of two-dimensional (2D) materials as promising candidates for next-generation electronic devices have been discovered and studied due to their unique electrical, mechanical, and optical properties.[1–4] Because of their appropriate band gap, 2D transition metal dichalcogenides (TMDs) are promising for future applications in the field of low-power logic devices, in which the short channel effects will be suppressed, the source–drain subthreshold leakage will be substantially reduced, and a high ON/OFF ratio will be obtained.[5,6] For example, monolayer MoS_2 based field effect transistors (FETs) have been demonstrated with a current ON/OFF ratio of $\sim 10^8$, a low subthreshold swing of 74 meV per decade, and a negligible OFF current of 25 fA μm^{-1}.[7] The contact interfaces between metallic electrodes and semiconductors are crucial to the electrical properties of devices.[8–13] Surface perturbation and reconstruction might lead to surface states within the band gap of semiconductors and disordered atomic structures at the semiconductor/metal interface. In addition, chemical disorder as well as defect-induced gap states could be produced, dependent on the integration and fabrication processes of devices. For example, TiO_2 rather than Ti might be formed at the interface if Ti is deposited on MoS_2 under a high vacuum of $\sim 1 \times 10^{-6}$ mbar, but Mo_xS_y, Ti_xS_y and metallic Mo could be produced at the interface with higher contact resistance if Ti is deposited under an ultrahigh vacuum of $\sim 1 \times 10^{-9}$ mbar.[14] Although a great number of research works have been focused on studying the interface between the gate dielectric layer and the 2D semiconductors, only a few research works have been focused on the contact interface between the metal and the 2D semiconductors at the source and drain electrodes.[15,16]

High contact resistance is still the critical factor limiting the high performance of 2D semiconductor based devices, which is mainly due to the wide contact tunnel barrier and the high

[a] State Key Laboratory for Mechanical Behavior of Materials, Xi'an Jiaotong University, Xi'an 710049, Shaanxi, China. E-mail: mafei@mail.xjtu.edu.cn
[b] College of Materials Science and Engineering, Shaanxi Normal University, Xi'an 710062, Shaanxi, China
[c] College of Physics and Information Technology, Shaanxi Normal University, Xi'an 710062, Shaanxi, China
[d] Department of Physics and Opt-electronic Engineering, Xi'an University of Arts and Science, Xi'an 710065, Shaanxi, China

† Electronic supplementary information (ESI) available. See DOI: 10.1039/c8tc04341h

Schottky barrier between metal and 2D materials.[17–20] So, the Schottky barrier height (SBH) is an important parameter to evaluate the electrical contact properties of devices.[21,22] In Schottky–Mott theory, the SBH is commonly determined by the work function of the contact metals. The work function of Sc, Ti, Cr, Ni, Au, Pd, and Pt is in a wide range, but the SBHs between the 2D semiconductors and these metals are weakly dependent on the work function of the metals owing to complex Fermi level pinning effect,[17,23] and high contact resistance is induced.[17] With respect to three-dimensional (3D) semiconductors, such as, Si, Ge, and III–V compounds, 2D semiconductors have a few dangling bonds on the pristine surface and do not tend to form covalent bonds, so 2D semiconductors stacked on the metals interact with each other through weak van der Waals (vdW) forces, of which an additional ''tunnel barrier'' besides the inherent Schottky barrier will be produced for carriers.[24] This tunnel barrier blocks the charge injection from metals greatly, resulting in higher contact resistance. For example, the contact resistance of monolayer MoS_2 on metals is up to 1 MΩ μm, which is more than 30 times higher than that of Si-based devices.[25,26] The right choice of metal contact in the fabrication of an electronic device is a key step towards low contact resistance, which is necessary to reduce power loss and to improve carrier injection efficiency across the interface. Kang *et al.*[24] and Pan *et al.*[27] have performed a comprehensive *ab initio* study on the interfacial properties of TMDs contacted with metals in the top contact configuration and offered guidance for the choice of suitable metal electrodes in TMD-based devices. As is well known, the interfacial states and properties of TMD/metal are dependent on the metal electrode and contact types. Kang *et al.*[24] analyzed the charge densities and electronic states in the interface regions, and they deduced that the edge contact configuration can be highly advantageous as compared to the top contact configuration in terms of the electron injection efficiency. However, Çakır *et al.*[28] found that the top contact configuration appears to be more advantageous as compared to the edge contact configuration in the case of monolayer $MoSe_2$ contacted with Sc electrodes. These inconsistent results puzzle us in selecting the metal contacts for electronic devices. Therefore, a thorough investigation on the influences of metal electrodes and contact modes as well as a quantitative understanding on the underlying physics is highly desirable.

In this paper, taking monolayer MoS_2 as an example, first-principles calculations have been done to study the interfacial electronic states and properties of 2D semiconductors contacted with metals (Mg, Al, In, Cu, Ag, Au, Pd, Sc, and Ti) in the top and edge contact configurations. It is found that the electronic states and the SBHs are extremely sensitive to the contact configurations and are metal dependent. The top contact configuration is preferred for the Sc/monolayer MoS_2 system as a result of an extremely low Schottky barrier (0.086 eV) as compared to that (0.439 eV) in the edge contact configuration, however, the edge contact configuration is preferred for Ag, Cu, Au, and Pd electrodes. This is consistent with the reported results of monolayer MoS_2/Sc (Au) systems.[17,26] Furthermore, metal electrodes in the top contact configuration usually result in n-type doping of monolayer MoS_2, but lead to strong p-type doping in the edge contact configuration. The results are discussed according to the changes in electronic states.

2. Computational method and model

The calculations are performed using the Vienna ab initio simulation package (VASP) based on density functional theory.[29,30] The electron–ion core interaction is described by the projector augmented wave potentials,[31] which are more accurate than the ultra-soft pseudo-potentials. The Perdew–Burke–Ernzerhof[32] formulation of the generalized gradient approximation is chosen to describe the exchange–correlation interaction. The DFT-D2 approach in the Grimme scheme is adopted to include the contribution from the vdW interaction between layers.[33] The cutoff energy for the plane-waves is chosen to be 400 eV. The Brillouin-zone integration is performed by using an $11 \times 11 \times 1$ k-mesh according to the Monkhorst–Pack scheme and a Gaussian smearing broadening of 0.2 eV is adopted. A conjugate-gradient algorithm is employed to relax the ions to the ground states with an energy convergence of 1.0×10^{-5} eV and a force convergence of 0.02 eV Å^{-1} on each ion, respectively. Chemical disorder and strong metallization commonly occur at the interfaces of TMDs/metal. Although the spin–orbit coupling significantly affects the electronic states and leads to the energy band splitting for the free-standing TMDs, the effects are negligible for TMD/metal interfaces because of the strong Fermi level pinning effect. Thus, the influences of spin–orbit coupling on the SBHs are negligible and it is not considered herein. Visualizations of supercells and structures are done using the VESTA software.[34]

The interface regions of monolayer MoS_2/metal are modeled, in which periodic conditions are applied in the x and y directions and separated by a vacuum of 15 Å in thickness along the z direction. Taking into account the structural stability, the crystal planes of different indexes are involved, that is, the (0001) plane for Mg, Al, Sc, and Ti, the (111) plane for Cu, Ag, Au and Pd, and the (101) plane for In. For the top contact configuration, monolayer MoS_2 is stacked on metals with six layers cut from the bulk to model the surface. Because of the different lattice constants of the metals as well as that of monolayer MoS_2 (a = 3.190 Å),[35] the supercells of the coincidence site lattice (CSL) in the commensurable structures are commonly different. The in-plane supercells are constructed to minimize the lattice misfit strain between monolayer MoS_2 and the metals,[36,37] in which a basis vector on a given metal surface is denoted by $n_1\vec{a}_1 + n_2\vec{a}_2$, with $(\vec{a}_1, \vec{a}_2)$ being the basis vectors of the primitive cell, and (n_1, n_2) the integers; similarly, $m_1\vec{b}_1 + m_2\vec{b}_2$ is a basis vector of the MoS_2 supercell, with $(\vec{b}_1, \vec{b}_2)$ being the basis vectors of the primitive cell, and (m_1, m_2) the integers. A set of values of n_1, n_2, m_1, and m_2 are found so that the lattice mismatch δ between the supercells of monolayer MoS_2 and the metals meets the following condition:

$$-\delta \leq \frac{|n_1\vec{a}_1 + n_2\vec{a}_2| - \left|m_1\vec{b}_1 + m_2\vec{b}_2\right|}{\left|m_1\vec{b}_1 + m_2\vec{b}_2\right|} \leq \delta. \quad (1)$$

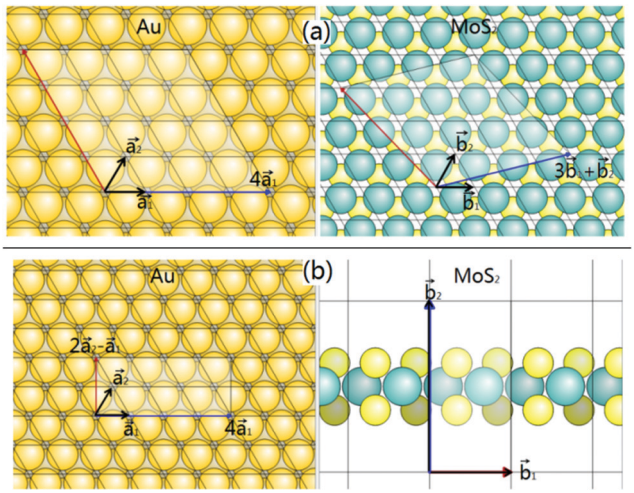

Fig. 1 Top view of Au (111) and monolayer MoS_2 surfaces indicating supercell structures: (a) top contact and (b) edge contact. The primitive basis vectors $\vec{a}_1$, $\vec{a}_2$ and $\vec{b}_1$, $\vec{b}_2$ of the Au (111) and MoS_2 lattices, respectively.

The $\sqrt{N} \times \sqrt{N}$ unit cell of a given metal is adjusted to the $\sqrt{M} \times \sqrt{M}$ unit cell of MoS_2, in which $N = n_1^2 + n_2^2 + n_1n_2$ and $M = m_1^2 + m_2^2 + m_1m_2$. For the in-plane lattice mismatch within δ ($\delta = 5\%$), the supercells of the contact heterostructures are usually large with broken symmetry. Fig. 1a as an example displays the supercell of Au on monolayer MoS_2.[37] In this way, the CSLs of given metals and monolayer MoS_2 are modeled, and the parameters are listed in Table 1 and the atomic structures are shown in Fig. S1 (ESI†). In order to construct the edge contact configuration, the monolayer MoS_2 nanoribbon is cut, as shown in Fig. S2 (ESI†), and an average length of $a > 10$ Å and $c > 15$ Å is simulated for the monolayer MoS_2 nanoribbon along the x and z directions, respectively. In the edge contact configuration, the lattice constant of the metals can be adjusted to those of the MoS_2 nanoribbon along the y direction, that is, $b = 5.474$ Å and $b = 3.190$ Å for armchair and zigzag terminations, respectively. As an example, Fig. 1b displays the supercells of rectangular Au contacted with the monolayer MoS_2 nanoribbon from the armchair termination. The CSLs of metals contacted with monolayer MoS_2 through Mo and S atoms at the armchair edges and that through Mo atoms at the zigzag edges are modeled, and the parameters are listed in Table 2 and the specific atomic structures are shown in Fig. S3 and S4 (ESI†).

Table 1 In-plane supercell defined by the MoS_2 basis vector $m_1\vec{b}_1 + m_2\vec{b}_2$ and the metal basis vector $n_1\vec{a}_1 + n_1\vec{a}_2$ for monolayer MoS_2 contacted with metals in the top contact configuration. δ represents the mismatch between the MoS_2 and metal lattices

	m_1, m_2	n_1, n_2	δ (%)
Mg	1, 0	1, 0	1
Al	1, 1	2, 0	1.09
In	4, 0	1, 0	4.15
Cu	5, 0	5, 0	0.73
Ag	4, −1	4, 0	0.93
Au	4, −1	4, 0	0.81
Pd	1, 1	2, 0	0.34
Sc	1, 1	1, 1	3
Ti	1, 1	1, 1	4.74

Table 2 In-plane supercell defined by the MoS_2 basis vector $m_1\vec{b}_1 + m_2\vec{b}_2$ and the metal basis vector $n_1\vec{a}_1 + n_2\vec{a}_2$ for monolayer MoS_2 contacted with metals in edge contact configurations through Mo and S atoms at armchair edges and Mo atoms at zigzag edges. δ is the mismatch between monolayer MoS_2 and metals

Through Mo and S atoms				Through Mo atoms			
	m_1, m_2	n_1, n_2	δ (%)		m_1, m_2	n_1, n_2	δ (%)
Mg	1, 0	1, 1	0.51	Mg	1, 0	1, 0	0.51
Al	1, 0	2, 0	3.30	Al	3, 0	2, 2	1.85
In	1, 0	−1, 2	2.50	In	2, 0	−1, 2	2.94
Cu	1, 0	2, 0	2.36	Cu	4, 0	5, 0	0.36
Ag	1, 0	2, 0	1.80	Ag	5, 0	4, 2	3.29
Au	1, 0	2, 0	1.71	Au	4, 0	4, 1	2.05
Pd	1, 0	2, 0	2.53	Pd	3, 0	2, 2	2.54
Sc	1, 0	1, 1	1.61	Sc	1, 0	1, 0	1.50
Ti	1, 0	2, 1	2.42	Ti	1, 0	1, 0	2.37

The atomic structures of metals contacted with monolayer MoS_2 though S atoms at the zigzag edges are not shown due to the similar atomic structure to that contacted through Mo atoms at the zigzag edges.

3. Results

After structural optimization, the most stable atomic configurations of monolayer MoS_2/metal contacts are obtained. Fig. 2 shows the optimized atomic structures in the top contact configuration. The relative positions of monolayer MoS_2 with respect to the metals are metal dependent, and the equilibrium distance between them, d, is defined as the average separation between the top metal layer and the bottom S layer of monolayer MoS_2. Accordingly, there are three types of contact interfaces: (1) very weak interaction, (2) medium interaction, and (3) strong interaction.[24] For the first one, no chemical bonds exist between metal atoms and monolayer MoS_2 due to a large interface separation, but the chemical bonding is enhanced gradually for the second and third ones as a result of reduced interface separation. The d values are 2.645, 2.701, and 2.884 Å for monolayer MoS_2 on Mg, Al, and In, respectively, and they are longer than the covalent bond lengths of Mg–S (2.46 Å), Al–S (2.26 Å), and In–S (2.47 Å) pairs,[38] respectively, indicating weak interaction between them. The d values are 2.312, 2.558, and 2.586 Å for monolayer MoS_2 on Cu, Ag, and Au, respectively, and they are comparable with the covalent bond lengths of Cu–S (2.37 Å), Ag–S (2.50 Å), and Au–S (2.41 Å),[39] respectively, indicating medium interaction between them. The d values are 2.225, 1.764, and 1.549 Å for Pd, Sc, and Ti on monolayer MoS_2, respectively, and they are shorter than the covalent bond lengths of Pd–S (2.44 Å), Sc–S (2.75 Å), and Ti–S (2.65 Å),[38] respectively, indicating strong interaction between them. However, for monolayer MoS_2 contacted with metals in the edge contact configuration, the bond length of metal–Mo (metal–S) in the interface becomes shorter than the covalent bond length, indicating strong chemical bonds between them (Tables S1–S3, ESI†). The bond length of Mo–S at the interface is also influenced by the strong interaction.

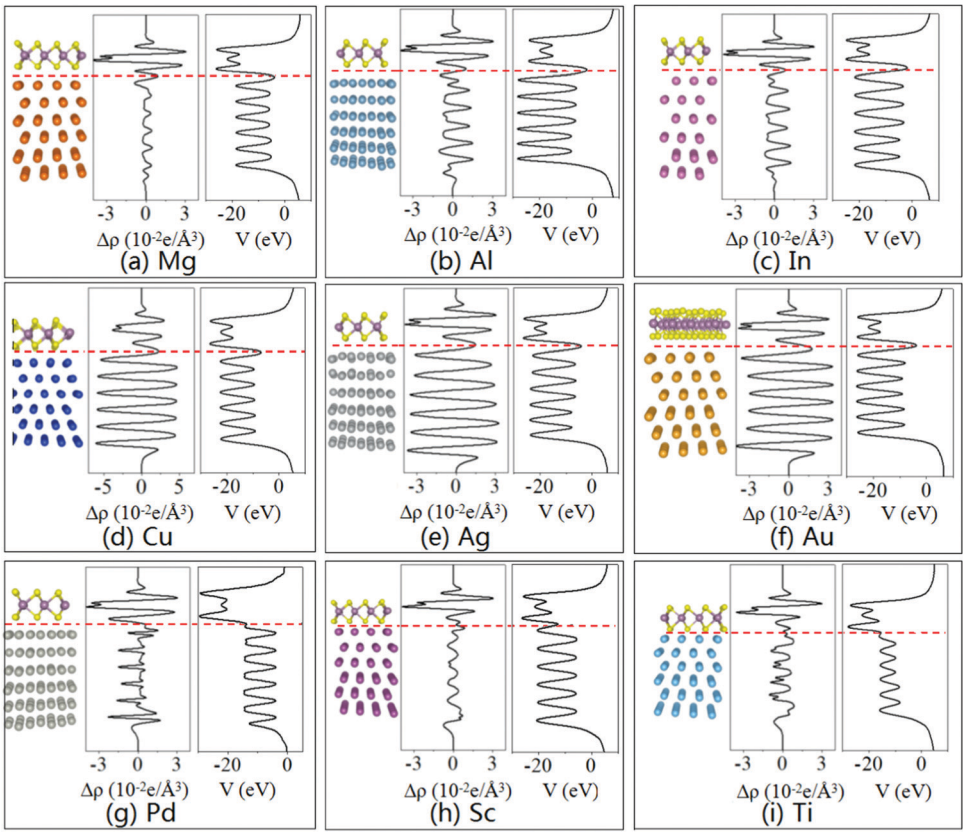

Fig. 2 Side view of the atomic structure, the charge density difference, and average electrostatic potential of monolayer MoS_2 on metals in the top contact configuration.

The interaction is also analyzed using the charge redistribution at the interface, of which a large charge density indicates a strong overlap of electron orbitals and sufficient injection of electrons into monolayer MoS_2.[7] The charge density difference is calculated as:

$$\Delta\rho(z) = \int \rho_{MoS_2-metal} dxdy - \int \rho_{MoS_2} dxdy - \int \rho_{metal} dxdy, \quad (2)$$

in which $\rho_{MoS_2\text{-metal}}$, ρ_{MoS_2}, and ρ_{metal} are the charge densities of the contact system, the isolated monolayer MoS_2, and the isolated metal, respectively. Fig. 2 displays the charge density difference of monolayer MoS_2 contacted with metals in the top contact configuration and the charge transfer at the interface is evidenced. Charge transfer oscillation occurs near the interface of monolayer MoS_2 on Sc/Ti, indicating strong interaction and the formation of interfacial dipole layers.[39,40] The strong interfacial interaction owing to orbital overlapping might promote the injection of electrons from the metal electrodes to the channels, and thus the tunneling and Schottky barriers will be lowered. The tunneling barrier ΔV is defined as the difference between the highest average potential at the contact interface and that at the metal surface,[41] and the values of ΔV are pseudo-potential and exchange–correlation function dependent.[42] At the strongly hybridized interfaces, for instance, the ΔV values for monolayer MoS_2 on Pd, Sc, and Ti are 0.294, −7.154, and −5.484 eV, respectively, suggesting that the electrons can be easily injected from the metal electrodes into monolayer MoS_2. While the ΔV values for monolayer MoS_2 on Mg, Al, In, Cu, Ag, and Au are 1.553, 4.365, 1.553, 2.770, 2.353, and 4.029 eV, respectively, indicating that there are tunneling barriers for electron injection, and they are consistent with the calculated values obtained by using the quantum transport simulations.[43] So Pd, Sc, and Ti might be the ideal electrode materials if they are contacted with monolayer MoS_2 in the top contact configuration.

However, it is a different case if monolayer MoS_2 is contacted with the metals in the edge contact configuration because there are unsaturated atoms at the edges, and strong hybridization usually occurs at the contact interfaces. As shown in Fig. 3a, the charge densities at the interface of the edge contact configurations are larger than that of the top contact configurations by more than 500%, demonstrating strong chemical bonding between monolayer MoS_2 and the metals. This can also be evidenced from the charge density difference, for example, a large charge density is accumulated at the interface when MoS_2 is contacted with either Mg or Sc in the edge contact configuration, but the similar case only occurs for monolayer MoS_2 contacted with Sc in the top contact configuration (Fig. 3b and c). Fig. 4 displays the average electrostatic potential of monolayer MoS_2 contacted with metals in the edge contact configuration. The average value increases from metals to MoS_2 at the interface gradually due to the charge transfer between them, and no tunneling barrier appears.

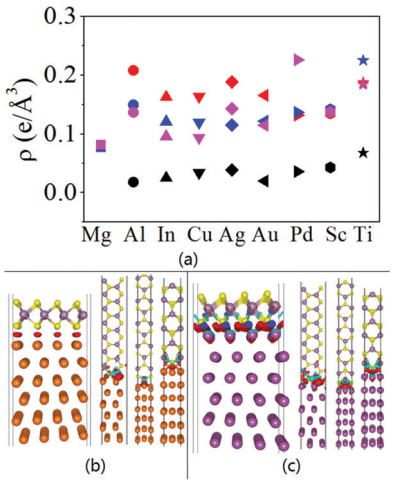

Fig. 3 (a) Total charge in the interface of monolayer MoS_2/metals. The black, red, blue, and magenta colors are used to denote the results in the top contact configuration, edge contact configurations through Mo and S atoms at the armchair termination, Mo atoms at the zigzag termination, and S atoms at the zigzag termination, respectively. (b) and (c) Charge density difference of MoS_2 contacted with Mg and Sc, respectively. The red and turquoise isosurfaces represent gain and depletion of charge density of 0.005 e Å^{-3}.

Fig. 5 displays the total and partial density of states (DOS) of monolayer MoS_2 contacted with metals in the top contact configuration. As compared with perfect monolayer MoS_2, the DOS changes little when it is contacted with Mg, Al, In, Cu, Ag, and Au in the top contact configuration. This confirms the weak interaction between them. There are no electronic states near the Fermi level E_F, characteristic of semiconductors. However, some electronic states emerge near the Fermi level E_F, characteristic of metallic features, if monolayer MoS_2 is contacted with Pd, Sc, and Ti. For the top contact configuration, half of the sulphur atoms are located at the interface, and they are denoted as S_b; the sulphur atoms far away from the interface are denoted as S_{nb}. The DOSs of the S_b and S_{nb} atoms are similar to each other, that is, independent of the position of the S atom. As an example, the PDOSs projected on each Mo and S atom of the MoS_2 nanoribbons contacted with Au electrodes in the edge contact configuration are calculated, and the results are shown in Fig. S5 (ESI†). It is found that only the PDOSs of the first-row Mo(S) atoms closest to the Au electrode are distinctly different from those in perfect single-layer MoS_2, but the PDOSs of the other Mo(S) atoms are almost the same as those in perfect single-layer MoS_2. So, the first-row Mo(S) atoms closest to the Au electrodes are defined as the interfacial Mo(S) atoms and marked by the number "(1)" in Fig. S5 (ESI†), and they are denoted by $Mo_b(S_b)$, and the other Mo(S) atoms are defined as the inner atoms and denoted by $Mo_{nb}(S_{nb})$. Generally, the metallized first-row Mo(S) atoms at the interface and the metal electrode are considered as a whole, and the electronic states, conduction band minimum (CBM) and valence band maximum (VBM) of the MoS_2 nanoribbons as well as the Schottky barrier with the metal electrodes are analyzed and discussed upon exclusion of the metallized first-row Mo(S)

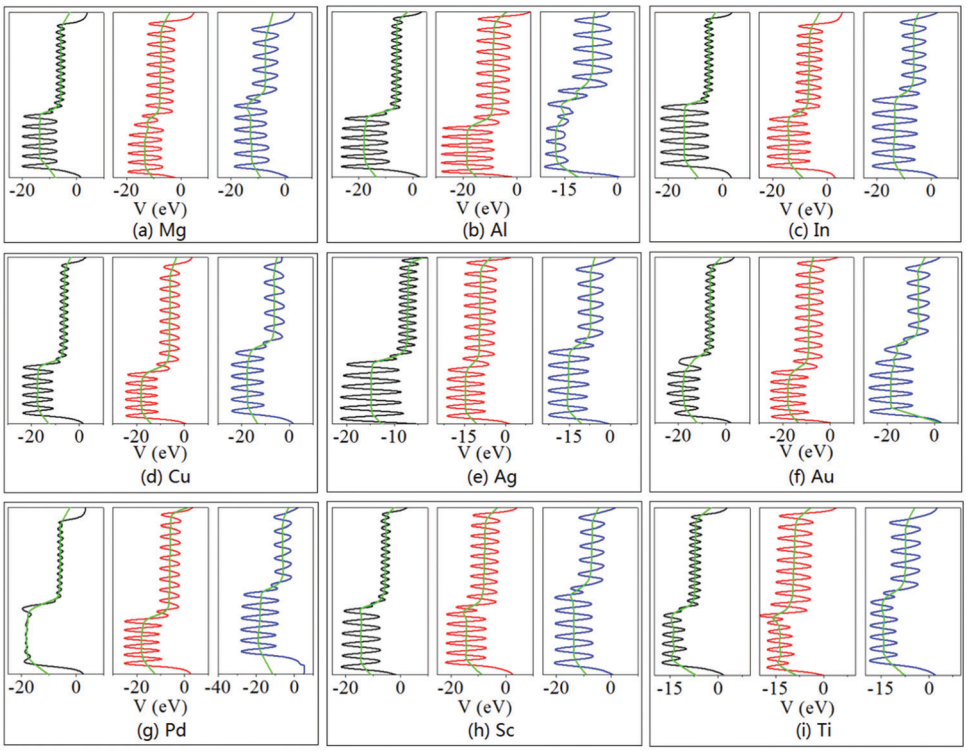

Fig. 4 Average electrostatic potential of monolayer MoS_2 contacted with metals in edge contact configurations. The black, red, and blue lines are used to denote the edge contact configuration through Mo and S atoms at the armchair termination, Mo atoms at the zigzag termination, and S atoms at the zigzag termination, respectively. The green line represents the average value.

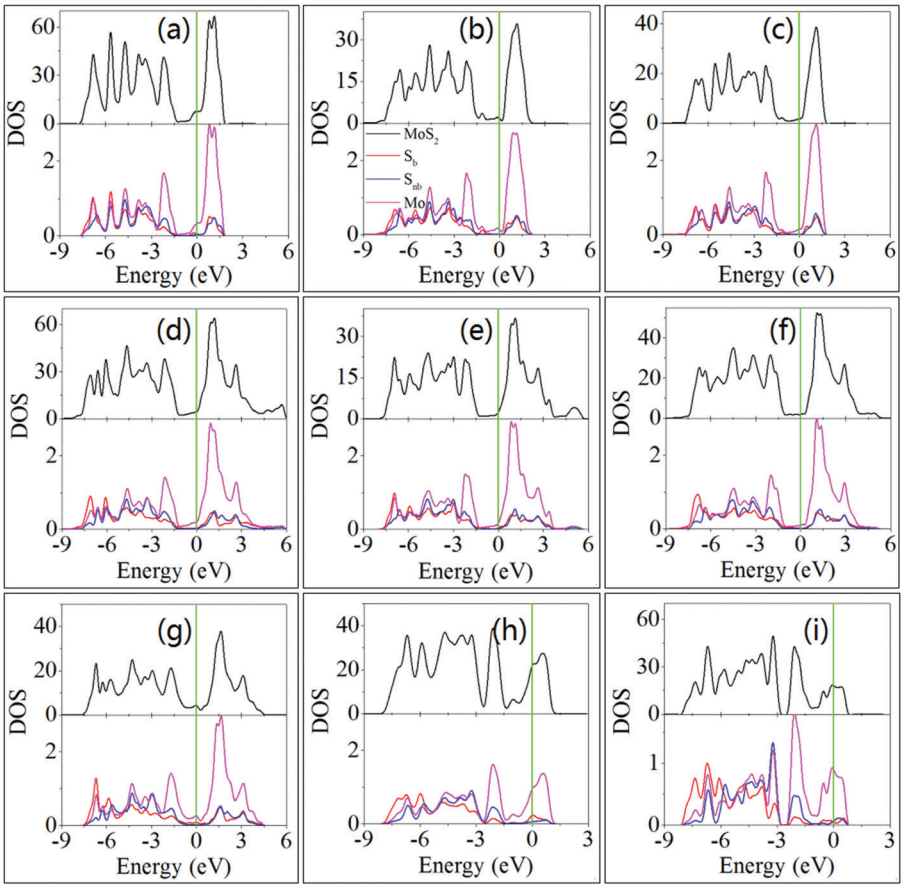

Fig. 5 Total and partial density of states (DOS) of monolayer MoS_2 contacted with metals in the top configuration: (a) Mg, (b) Al, (c) In, (d) Cu, (e) Ag, (f) Au, (g) Pd, (h) Sc, and (i) Ti. S_b (red line) and S_{nb} (blue line) are the sulphur atoms at the interface and far away from the interface, respectively, and Mo (magenta lines) is the molybdenum atom in monolayer MoS_2 on metals.

atoms at the interface. Furthermore, the electronic states of the MoS_2 nanoribbons with different widths along the z direction are calculated to study the influences of the nanoribbon width on the contact properties in the edge contact configuration. As shown in Fig. S6 (ESI†), the DOSs are almost coincident with each other, independent of the nanoribbon width. So, the armchair (zigzag) MoS_2 nanoribbons with a width of about 21.2 Å (26 Å) and contacted with Au electrodes in the edge contact configuration are adopted as an example. Wang *et al.*[44] found that the band gap of the armchair MoS_2 nanoribbon changes with increasing ribbon width but converges to 0.544 eV at the ribbon width of 12 ($N \geq 12$). However, the armchair MoS_2 nanoribbons with widths larger than 21.2 Å ($N \geq 14$) are adopted in our calculations, and the width dependence of the band gap is negligible. In addition, taking into account the enormous computational source required, the nanoribbon width along the y direction cannot be changed into a large value, and thus the periodic condition is adopted along the y direction and the influence of the ribbon width along this direction is not considered herein. Interestingly, in spite of the strong interaction between MoS_2 and metals in the edge contact configuration, the DOS is quite similar to that of pristine monolayer MoS_2 (Fig. 6 and Fig. S7, S8, ESI†). In the edge contact configuration with the zigzag termination, only one MoS_2 unit is bonded with the metals, so the interfacial effect on the electronic states of MoS_2 is negligible as a whole, although the electronic states of Mo and S atoms (Mo_b and S_b) at the interface are significantly perturbed. The electronic states near the Fermi level originate mainly from the Mo_b atom but also a little from the S_b atom (Fig. 6). Evidently, the electronic states of Mo and S atoms (Mo_{nb} and S_{nb}) far away from the interface are hardly affected.

The tunnel and Schottky barriers are crucial to the device performances. As shown in Fig. 7, the n-type Schottky barrier is indeed the energy difference of the CBM with respect to the Fermi level E_F, while the p-type Schottky barrier is indeed the energy difference of the VBM with respect to the Fermi level E_F. As for monolayer MoS_2 contacted with metals in the top contact configuration, the Fermi level E_F is pinned close to the CBM, characteristic of n-type Schottky barriers. The barrier height $\Phi_{SB,N}$ of monolayer MoS_2 contacted with Al, In, Mg, Ag, Au, Cu, and Pd in the top contact configuration is 0.212, 0.248, 0.260, 0.405, 0.440, 0.537, and 0.729 eV, respectively. But, the SBH could not be properly determined for monolayer MoS_2 contacted with Sc and Ti in the top contact configuration because monolayer MoS_2 almost changed into a metal as a result of the strong interaction between them. Lu *et al.*[45] and Lee *et al.*[46]

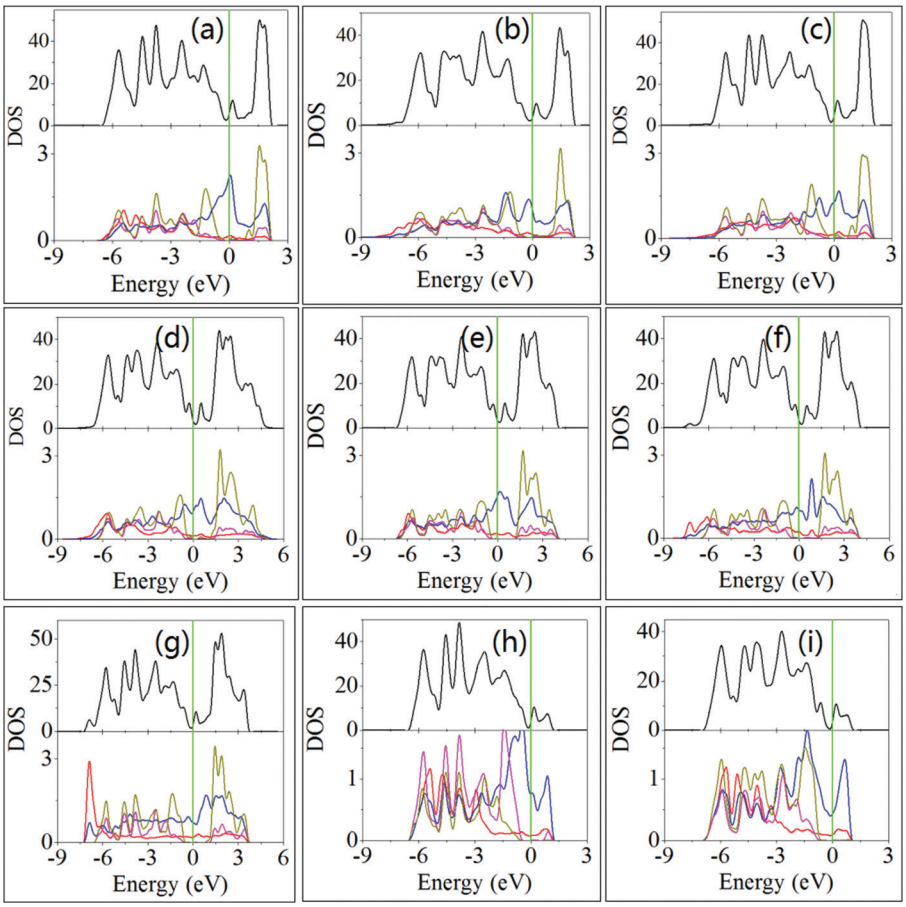

Fig. 6 Total (up panel) and partial (down panel) DOS of monolayer MoS_2 contacted with metals in the edge contact configuration through Mo and S atoms at the armchair termination: (a) Mg, (b) Al, (c) In, (d) Cu, (e) Ag, (f) Au, (g) Pd, (h) Sc, and (i) Ti. S_b (red line) and S_{nb} (magenta line) are the sulphur atoms at the interface and far away from the interface, respectively. Similarly, Mo_b (blue line) and Mo_{nb} (dark yellow line) are the molybdenum atoms at the interface and far away from the interface, respectively.

reported that the SBH between *N*-layer 2D semiconductors and strongly interacted metals might be estimated from the electronic states of the $(N + 1)$-layer counterpart. Hence, the electronic structures of bilayer MoS_2 contacted with Sc and Ti on the top were calculated to estimate the SBH of the monolayer counterparts. The $\Phi_{SB,N}$ values of MoS_2 contacted with Sc and Ti in the top contact configuration are 0.086 and 0.411 eV, respectively. Moreover, the previously reported experimental and theoretical SBH values are listed in Table S4 (ESI†) for comparison. Liu *et al.* obtained the small SBH value of 0.06 eV if Au electrodes are directly deposited on MoS_2 in a top contact configuration.[47] Kim *et al.*[23] found the large SBH value of 0.32 eV when MoS_2 is stamped onto pre-patterned Au electrodes. Kang *et al.*[24] and Dong *et al.*[48] illustrated the bipolar characteristics of MoS_2 on Pd. The prediction of the n-type Schottky contact of ours is confirmed by the calculations of Gong's group.[20] The differences between the experimental and theoretical results of SBH might be ascribed to the interfacial defects in the experimental samples and the different measurement conditions, which are not taken into account in theoretical calculations. This will be studied in detail in the future.

It is a completely different case for monolayer MoS_2 contacted with metals in the edge contact configuration. As mentioned above, only the PDOSs of $Mo_b(S_b)$ atoms at the interface are characteristic of metallic features (Fig. 6 and Fig. S7, S8, ESI†), and the metallized $Mo_b(S_b)$ atoms and the metal electrode are generally considered as a whole. So, the Schottky barrier of MoS_2 contacted with the metal in the edge contact configuration can be obtained by analyzing the electronic states of Mo_{nb} and S_{nb} atoms in monolayer MoS_2. As shown in Fig. 7b–d, p-type Schottky barriers will be produced for MoS_2, except for that of MoS_2 contacted with Ti and Sc through S atoms at the zigzag termination. It should be noted that the Schottky barrier is the lowest ($\sim$0.3 eV) if monolayer MoS_2 is contacted with metals through Mo atoms at the zigzag termination, but it is highest ($>$0.5 eV) if monolayer MoS_2 is contacted with metals through S atoms at the zigzag termination. As for the MoS_2/Sc system, the Schottky barrier of the edge contact configuration is much higher than that of the top contact configuration. But, the Schottky barriers are reduced for monolayer MoS_2 contacted with Ag, Cu, Au and Pd in the edge contact configuration, especially for that contacted through Mo at the zigzag termination. So, the top contact configuration is highly preferred if Sc is used as the electrode in monolayer MoS_2 based devices, but the edge contact configuration is highly preferred

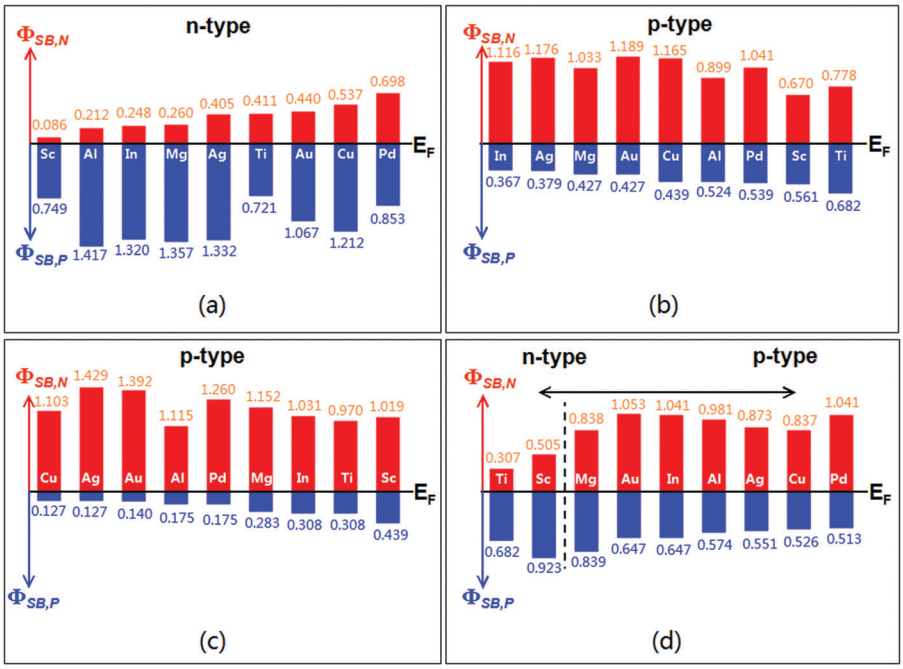

Fig. 7 Schottky barrier height (SBH) of monolayer MoS_2/metals: (a) top contact configuration, (b) edge contact configuration through contacting Mo and S atoms at armchair termination, (c) and (d) edge contact configuration through contacting Mo and S atoms at zigzag termination, respectively.

for Ag, Cu, Au, and Pd electrodes. Besides, an n-type Schottky contact will be formed for the top contact mode, but a p-type Schottky contact will be formed for the edge contact mode.

The pinning factor and the charge neutrality level were adopted to describe the Fermi level pinning effect.[49] According to the Schottky–Mott rule, the SBH for electrons ($\Phi_{SB,N}$) is given

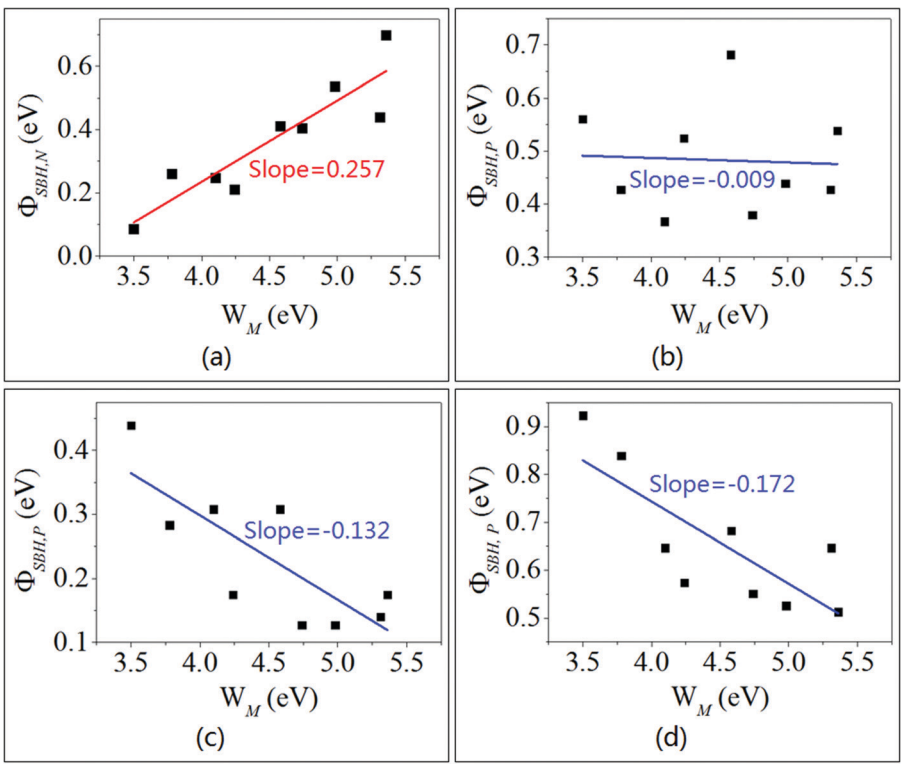

Fig. 8 SBH of monolayer MoS_2/metals as a function of work function of metals: (a) top contact configuration, (b) edge contact configuration through Mo and S atoms at armchair termination, (c) and (d) edge contact configuration through Mo and S atoms at zigzag termination, respectively.

by the difference between the work function of a metal (W_M) and the electron affinity of the semiconductor (χ):

$$\Phi_{SB,N} = W_M - \chi. \quad (3)$$

The n-type SBH is characterized by the pinning factor (S) and the charge neutrality level (CNL, Φ_{CNL}).

$$\Phi_{SB,N} = S(W_M - \Phi_{CNL}) + (\Phi_{CNL} - \chi) = SW_M + b. \quad (4)$$

These can be used as figures of merits calculated from the slope of the linear fitted line and the SBH. S is indeed the slope, $S = d\Phi_{SB,N}/dW_M$; $S = 1$ for an unpinned interface and $S = 0$ for a strongly pinned interface. The p-type SBH ($\Phi_{SB,P}$) decreases with increasing W_M,

$$\Phi_{SB,P} = \chi + E_g - W_M, \quad (5)$$

in which E_g is the band gap of the semiconductor. The sum of the electron affinity and the band gap is the VBM. The slope of the p-type Schottky barrier *vs.* W_M ($S = d\Phi_{SB,P}/dW_M$) will be -1 for the unpinned case. The pinning factor and Φ_{CNL} for the p-type SBH can be estimated as:

$$\Phi_{SB,P} = S(W_M - \Phi_{CNL}) + (\chi + E_g - \Phi_{CNL}) = SW_M + b. \quad (6)$$

Fig. 8 shows the Schottky barriers *vs.* W_M for monolayer MoS_2 contacted with metals. The calculated S value is 0.257 for monolayer MoS_2 contacted with metals in the top contact configuration, which is consistent with the reported theoretical value of 0.27.[50] Actually, the theoretical value is substantially larger than the experimental value of $S \sim 0.1$.[17,23] The difference might be due to the enhanced Fermi pining effect from the structural defects in the experimental samples. Both the experimental and theoretical results exhibit a strong p-type feature for monolayer $MoTe_2$ contacted with metals in the top contact configuration, and the Fermi level pinning effect is evidenced with the S values of -0.07 and -0.17, respectively.[23,51] Similar behaviors are observed for monolayer MoS_2 contacted with metals in the edge contact configurations, in which the S values of -0.009, -0.132, and -0.172 are obtained for MoS_2 contacted with metals in the edge contact configuration through Mo and S atoms at the armchair termination, Mo atoms at the zigzag termination, and S atoms at the zigzag termination, respectively. Therefore, the dipole moment in the MoS_2-based device can be modulated by changing the contact mode at the source and drain ends. Although the strong Fermi pinning effect in monolayer MoS_2 contacted with metals on the top might be suppressed through surface passivation and 2D material intercalation,[52,53] it is still challenging to weaken the Fermi pinning effect at the monolayer MoS_2–metal interface in the edge contact mode.

4. Conclusions

The influences of contact configurations on the interfacial electronic states between monolayer MoS_2 and metals (Mg, Al, In, Cu, Ag, Au, Pd, Sc, and Ti) are studied by using first-principles calculations. As for the Sc/monolayer MoS_2 system, the SBH (0.086 eV) is extremely low in the top contact configuration, and it is large (>0.439 eV) in the edge contact configuration, that is, the top contact configuration is preferred for such a system. However, the SBHs of monolayer MoS_2 contacted with Cu, Ag, Au, and Pd in the edge contact configuration are lower than those in the top contact configuration. The top contact configuration always exhibits n-type doping, but it is p-type for the edge contact configuration. Accordingly, the dipole moment could be modulated by changing the contact configurations for monolayer MoS_2 contacted with metals. Furthermore, a strong Fermi level pinning effect occurs in the monolayer MoS_2/metal contact. The results provide us with theoretical guidance for the selection of metals and contact modes for 2D material devices.

Conflicts of interest

There are no conflicts to declare.

Acknowledgements

This work was jointly supported by the National Natural Science Foundation of China (Grant No. 51771144, 51471130 and 51501012) and the Natural Science Foundation of Shaanxi Province (No. 2017JZ015). This work was carried out using the HPCC Platform at the Xian Jiaotong University.

References

1 A. K. Geim and K. S. Novoselov, *Nat. Mater.*, 2007, **6**, 183–191.
2 C. Lee, X. D. Wei, J. W. Kysar and J. Hone, *Science*, 2008, **321**, 385–388.
3 K. S. Kim, T. Zhao, H. Jang, S. Y. Lee, J. M. Kim, K. S. Kim, J.-H. Ahn, P. Kim, J.-Y. Choi and B. H. Hong, *Nature*, 2009, **457**, 706–710.
4 D. Jariwala, V. K. Sangwan, L. J. Lauhon, T. J. Marks and M. C. Hersam, *ACS Nano*, 2014, **8**, 1102–1120.
5 O. Lopez-Sanchez, D. Lembke, M. Kayci, A. Radenovic and A. Kis, *Nat. Nanotechnol.*, 2013, **8**, 497–501.
6 S. Jo, N. Ubrig, H. Berger, A. B. Kuzmenko and A. F. Morpurgo, *Nano Lett.*, 2014, **14**, 2019–2025.
7 B. Radisavljevic, A. Radenovic, J. Brivio, V. Giacometti and A. Kis, *Nat. Nanotechnol.*, 2011, **6**, 147–150.
8 J. Kang, D. Sarkar, W. Liu, D. Jena and K. Banerjee, *IEEE Int. Electron Devices Meet.*, 2012, 17.4.1–17.4.4.
9 I. Popov, G. Seifert and D. Tománek, *Phys. Rev. Lett.*, 2012, **108**, 156802.
10 H. Fang, M. Tosun, G. Seol, T. C. Chang, K. Takei, J. Guo and A. Javey, *Nano Lett.*, 2013, **13**, 1991–1995.
11 H. Fang, S. Chuang, T. C. Chang, K. Takei, T. Takahashi and A. Javey, *Nano Lett.*, 2012, **12**, 3788–3792.
12 W. Liu, J. Kang, D. Sarkar, Y. Khatami, D. Jena and K. Banerjee, *Nano Lett.*, 2013, **13**, 1983–1990.
13 C. D. English, G. Shine, V. E. Dorgan, K. C. Saraswat and E. Pop, *Nano Lett.*, 2016, **16**, 3824–3830.

14 S. McDonnell, C. Smyth, C. L. Hinkle and R. M. Wallace, *ACS Appl. Mater. Interfaces*, 2016, **8**, 8289–8294.
15 R. Xie, T. H. Phung, M. B. Yu and C. X. Zhu, *IEEE Trans. Electron Devices*, 2010, **57**, 1399–1407.
16 K. Martens, C. O. Chui, G. Brammertz, J. B. De, D. Kuzum, M. Meuris, M. Heyns, T. Krishnamohan, K. Saraswat, H. E. Maes and G. Groeseneken, *IEEE Trans. Electron Devices*, 2008, **55**, 547–556.
17 S. Das, H. Y. Chen, A. V. Penumatcha and J. Appenzeller, *Nano Lett.*, 2012, **13**, 100–105.
18 W. Mönch, *Appl. Phys. Lett.*, 1998, **72**, 1899–1901.
19 H. Liu, M. Si, Y. Deng, A. T. Neal, Y. Du, S. Najmaei, P. M. Ajayan, J. Lou and P. D. Ye, *ACS Nano*, 2014, **8**, 1031–1038.
20 C. Gong, L. Colombo, R. M. Wallace and K. Cho, *Nano Lett.*, 2014, **14**, 1714–1720.
21 A. Allain, J. Kang, K. Banerjee and A. Kis, *Nat. Mater.*, 2015, **14**, 1195–1205.
22 F. Leonard and A. A. Talin, *Nat. Nanotechnol.*, 2011, **6**, 773–783.
23 C. Kim, I. Moon, D. Lee, M. S. Chio, F. Ahmed, S. Nam, Y. Cho, H.-J. Shin, S. Park and W. J. Yoo, *ACS Nano*, 2017, **11**, 1588–1596.
24 J. Kang, W. Liu, D. Sarkar, D. Jena and K. Banerjee, *Phys. Rev. X*, 2014, **4**, 031005.
25 B. W. H. Baugher, H. O. H. Churchill, Y. Yang and P. JarilloHerrero, *Nano Lett.*, 2013, **13**, 4212–4216.
26 S. Das and J. Appenzeller, *Nano Lett.*, 2013, **13**, 3396–3402.
27 Y. Y. Pan, S. B. Li, M. Ye, R. G. Quhe, Z. G. Song, Y. Y. Wang, J. X. Zheng, F. Pan, W. L. Guo, J. B. Yang and J. Lu, *J. Phys. Chem. C*, 2016, **120**, 13063–13070.
28 D. Çakır and F. M. Peeters, *Phys. Rev. B: Condens. Matter Mater. Phys.*, 2014, **89**, 245403.
29 G. Kresse and J. Hafner, *Phys. Rev. B: Condens. Matter Mater. Phys.*, 1993, **47**, 558–561.
30 G. Kresse and J. Hafner, *Phys. Rev. B: Condens. Matter Mater. Phys.*, 1994, **49**, 14251–14269.
31 P. E. Blöchl, *Phys. Rev. B: Condens. Matter Mater. Phys.*, 1994, **50**, 17953–17979.
32 J. P. Perdew, K. Burke and M. Ernzerhof, *Phys. Rev. Lett.*, 1996, **77**, 3865–3868.
33 S. Grimme, *J. Comput. Chem.*, 2006, **27**, 1787–1799.
34 K. Momma and F. Izumi, *J. Appl. Crystallogr.*, 2008, **41**, 653–658.
35 A. H. Reshak and S. Auluck, *Phys. Rev. B: Condens. Matter Mater. Phys.*, 2003, **68**, 125101.
36 H. P. Komsa and A. V. Krasheninnikov, *Phys. Rev. B: Condens. Matter Mater. Phys.*, 2013, **88**, 085318.
37 M. Farmanbar and G. Brocks, *Phys. Rev. B: Condens. Matter Mater. Phys.*, 2016, **93**, 085304.
38 B. Cordero, V. Gómez, A. E. Platero-Prats, M. Revés, J. Echeverría, E. Cremades, F. Barragán and S. Alvarez, *Dalton Trans.*, 2008, 2832–2838.
39 G. Giovannetti, P. A. Khomyakov, G. Brocks, V. M. Karpan, J. van den Brink and P. J. Kelly, *Phys. Rev. Lett.*, 2008, **101**, 026803.
40 H. Jin, J. W. Li, L. H. Wan, Y. Dai, Y. D. Wei and H. Guo, *2D Mater.*, 2017, **4**, 025116.
41 K. Gong, L. Zhang, W. Ji and H. Guo, *Phys. Rev. B: Condens. Matter Mater. Phys.*, 2014, **90**, 125441.
42 G. Kresse and D. Joubert, *Phys. Rev. B: Condens. Matter Mater. Phys.*, 1999, **59**, 1758.
43 H. X. Zhong, R. G. Quhe, Y. Y. Wang, Z. Y. Ni, M. Ye, Z. G. Song, Y. Y. Pan, J. B. Yang, L. Yang, M. Lei, J. J. Shi and J. Lu, *Sci. Rep.*, 2016, **6**, 21786.
44 R. Wang, X. Y. Zhou, X. Y. Xu, J. G. Hu and J. Pan, *J. Phys. D: Appl. Phys.*, 2017, **50**, 095102.
45 X. Y. Zhang, Y. Y. Pan, M. Ye, R. G. Quhe, Y. Y. Wang, Y. Guo, H. Zhang, Y. Dan, Z. G. Song, J. S. Li, J. B. Yang, W. L. Guo and J. Lu, *Nano Res.*, 2018, **11**, 707–721.
46 S. Y. Lee, W. S. Yun and J. D. Lee, *ACS Appl. Mater. Interfaces*, 2017, **9**, 7873–7877.
47 Y. Liu, J. Guo, E. B. Zhu, L. Liao, S. J. Lee, M. N. Ding, I. Shakir, V. Gambin, Y. Huang and X. F. Duan, *Nature*, 2018, **557**, 696–700.
48 H. Dong, C. Gong, R. Addou, S. McDonnell, A. Azcatl, X. Y. Qin, W. C. Wang, W. H. Wang, C. L. Hinkle and R. M. Wallace, *ACS Appl. Mater. Interfaces*, 2017, **9**, 38977–38983.
49 J. Robertson, *J. Vac. Sci. Technol., A*, 2013, **31**, 050821.
50 Y. Y. Wang, M. Ye, M. Y. Weng, J. Z. Li, X. Y. Zhang, H. Zhang, Y. Guo, Y. Y. Pan, L. Xiao, J. K. Liu, F. Pan and J. Lu, *ACS Appl. Mater. Interfaces*, 2017, **9**, 29273–29284.
51 Y. Z. Guo, D. M. Liu and J. Robertson, *ACS Appl. Mater. Interfaces*, 2015, **7**, 25709–25715.
52 K.-A. Min, J. Park, R. M. Wallace, K. Cho and S. Hong, *2D Mater.*, 2017, **4**, 015019.
53 J. Su, L. P. Feng, W. Zeng and Z. T. Liu, *Phys. Chem. Chem. Phys.*, 2016, **18**, 31092–31100.

